Importin α as a molecular marker for investigating the microenvironment of micronuclei

Yoichi Miyamoto[1,‡,*], Reo Kisanuki[2,‡], Rieko Oshima[1], Chiaki Hata[3], Taro Tachibana[3,4], Masahiro Oka[1], and Hisato Saitoh[2,5,*]

[1]Laboratory of Nuclear Transport Dynamics, Center for Drug Design Research, National Institutes of Biomedical Innovation, Health and Nutrition (NIBIOHN), Osaka, Japan.

[2]Department of Biological Science, Graduate School of Science and Technology, Kumamoto University, Kumamoto, Japan.

[3]Cell Engineering Corporation, Osaka, Japan.

[4]Department of Bioengineering, Graduate School of Engineering, Osaka Metropolitan University, Osaka, Japan.

[5]Faculty of Advanced Science and Technology (FAST), Kumamoto University, Kumamoto, Japan.

[‡]These authors contributed equally.

[*]Correspondence:

Y. Miyamoto, E-mail: ymiyamoto@nibiohn.go.jp; *Laboratory of Nuclear Transport Dynamics, Center for Drug Design Research, National Institutes of Biomedical Innovation, Health and Nutrition (NIBIOHN), 7-6-8 Saito-Asagi, Ibaraki-shi, Osaka 567-0085, Japan*

H. Saitoh, E-mail: hisa@kumamoto-u.ac.jp; *Faculty of Advanced Science and Technology (FAST), Kumamoto University, 2-39-1 Kurokami, Chuo-ku, Kumamoto 860-8555, Japan*

Running title: Importin α in micronuclei.

Keywords: Cancer development, Chromatin, DNA damage, Genome instability, Micronucleus, Nuclear transport

Summary statement: Accumulation of importin α in micronuclei, followed by alteration of their microenvironment, suggests the non-canonical function of importin α in genome instability and cancer development.

ABSTRACT

Micronuclei (MN) are nuclear membrane-enclosed cellular structures that contain DNA/chromatin fibers that can lead to genomic instability. Here, we report that importin α, known as the nuclear transport factor, is highly concentrated in some of the MN in cultured human cancer cells. We observed that importin α1 accumulated in the MN together with other subtypes, indicating that this represented a conserved feature of the importin α family. Indirect immunofluorescence analysis revealed that the MN localization of importin α1 was regulated independently of canonical nuclear transport-related factors such as importin β1, CAS/CSE1L, nucleoporins, and lamins. In contrast, importin α1 signals merged with histone H3 modified by trimethylation at lysine 4 in MN, indicating that importin α1 was associated with euchromatin in MN. Furthermore, we found a mutually exclusive relationship between importin α1 and RAD51, a homologous recombination repair protein, in relation to MN accumulation in cells exposed to etoposide, a DNA damaging reagent. Our findings suggest that importin α is a previously overlooked molecular marker for assessing the microenvironment and quality control of MN in human cancer cells.

INTRODUCTION

Micronuclei (MN) are cytoplasmic structures embedded within the nuclear envelope and are spatially separated from the primary nucleus. MN contain DNA/chromatin fibers, which are frequently observed in cancerous cells during senescence and after genotoxic stress (Hintzsche et al., 2017). This indicates a link between MN and genome instability, including chromosome rearrangements, mutagenesis, and chromothripsis (Krupina et al., 2021; Kwon et al., 2020; Zhang et al., 2015). In particular, the study of chromothripsis in many aggressive types of cancer has been rapidly expanding and advancing, suggesting that MN actively participates in chromothripsis during cancer development, progression, and genome evolution (Forment et al., 2012; Ly and Cleveland, 2017; Storchová and Kloosterman, 2016). Moreover, it was reported that the exposure of DNA/chromatin fibers within MN to cytoplasmic components served as a potent molecular pattern signal, by activating sterile inflammatory responses and inflammation in the absence of pathogenic infection, which are associated with many chronic age-associated conditions (Miller et al., 2021).

Importin α, also known as karyopherin α (KPNA), is a classical nuclear localization signal (cNLS) receptor that plays a crucial role in nuclear-cytoplasmic transport through nuclear pore complexes [NPCs; (Liu and Hetzer, 2022; Walde and Kehlenbach, 2010)] present in the nuclear envelope (Goldfarb et al., 2004). It acts as an adaptor molecule between a cNLS-bearing cargo and the carrier molecule importin β1 in the cytoplasm. The trimeric complex migrates into the nucleus depending on the Ras-like small GTPase Ran (Poon and Jans, 2005; Wente and Rout, 2010). After the complex dissociates in the nucleus by the binding of importin β1 and RanGTP, importin α is exported to the cytoplasm by cellular apoptosis susceptibility gene product CAS, also known as chromosome segregation 1-like [CSE1L; (Behrens et al., 2003; Stewart, 2007)]. Seven importin α subtypes have been identified in humans, including importin α1 (KPNA2), importin α3 (KPNA4),

71 importin α4 (KPNA3), importin α5 (KPNA1), importin α6 (KPNA5), importin α7 (KPNA6), and
72 importin α8 (KPNA7), which exhibit distinct cNLS-binding specificities and selective expression
73 in various tissues (Goldfarb et al., 2004; Pumroy and Cingolani, 2015).

74 In addition to their role in the nuclear-cytoplasmic transport regulation, importin αs also
75 have non-transport roles such as regulation of spindle assembly, lamin polymerization, nuclear
76 envelope formation, protein degradation, stress response, gene expression, cell surface response,
77 and mRNA metabolism (Miyamoto et al., 2016; Oka and Yoneda, 2018), emphasizing their multi-
78 functionality. Importin αs were observed to accumulate in the nucleus under special occasions and
79 environments such as in stress responses, wherein they bind to a DNase-sensitive nuclear
80 component, indicating their potential to associate with DNA/chromatin (Furuta et al., 2004; Kodiha
81 et al., 2008; Miyamoto et al., 2004). Indeed, we have previously demonstrated that the nuclear-
82 localized importin α could associate with chromatin and regulate its gene expression (Yasuda et al.,
83 2012). In addition, a recent report implied that the importin β binding (IBB) domain was
84 responsible for the DNA binding of importin α (Jibiki et al., 2021). These findings have suggested
85 that the nuclear-localized importin α can function as a regulator for nuclear homeostasis through
86 its intrinsic activity to bind to DNA/chromatin.

87 Evidence reveals that importin αs are highly expressed in various cancers (Christiansen and
88 Dyrskjot, 2013; Stelma et al., 2016). Among these, importin α1/KPNA2 has been well investigated,
89 and its high expression levels were associated with poor prognoses in cancer cells (Han and Wang,
90 2020; Sun et al., 2021; Wang et al., 2012). Notably, strong nuclear staining of importin α1 was
91 observed in breast cancer using immunohistochemical analysis and was extensively associated
92 with a higher tumor stage (Alshareeda et al., 2015; Dahl et al., 2006; Dankof et al., 2007).

93 In this study, we investigated the dynamics and functions of importin α in several human
94 cancer cell lines, including HeLa, MCF7, and MDA-MB-231. We discovered a considerable

95 concentration of importin αs, although not all, in MN. Our findings indicate that the MN-
96 localization of importin α does not fully align with its conventional role as a nuclear transport factor.
97 We also identified and characterized several potential candidate nuclear/chromatin proteins linked
98 to importin α1 function, providing not only a new molecular marker of MN but also hints to
99 elucidate the MN structure and quality control in cancerous cells.
100

101 **RESULTS**

102 **Visualization of importin α accumulation in micronuclei**

103 Previous studies have reported that importin α was highly expressed and localized in the nucleus
104 of various cancer cells, suggesting a potential association between higher tumor stage and patient
105 survival (Christiansen and Dyrskjot, 2013; Han and Wang, 2020). To clarify the enhanced
106 expression of importin α subfamilies in cancerous cell lines, we performed a western blot assay
107 using breast cancer cell lines (MCF7, MDA-MB-231, and SK-BR-3), along with a control cell
108 line (MCF10A). Our data indicated that importin αs, particularly importin α1 (KPNA2), were
109 expressed at higher levels in cancer cell lines (Fig. S1).

110 To further investigate the localization of importin α, we performed indirect
111 immunofluorescence (IF) analyses using antibodies against importin α1 in human cancer cell lines
112 (MCF7 and HeLa cells). We found that a substantial number of micronuclei (MN) exhibited
113 stronger signals than the primary nuclei (PN), although not all MN showed this pattern (Fig. 1A,
114 yellow arrowhead). The fluorescence intensity of PN was considerably lower than that of MN,
115 suggesting an increased efficiency of importin α1 transport and/or maintenance in a subset of MN
116 compared with PN (Fig. 1B). We categorized the signal patterns in MN into three groups, based
117 on the IF analyses using the anti-importin α1 antibody: high intensity (yellow arrowhead), low
118 intensity (white arrowhead), or no intensity (white arrow) (Fig. 1C). The three patterns of importin
119 α1 accumulation in MN were also observed in HeLa cells treated with reversine, a mitotic aurora
120 kinase inhibitor that efficiently induces MN [Fig. S2; (Miyazaki et al., 2020)]. Among the MN
121 observed in HeLa cells, approximately 30% exhibited high intensity and 10% exhibited low
122 intensity, indicating that up to 40% of MN showed importin α1 accumulation under our standard
123 culture conditions as well as reversine treatment (Fig. 1D). We also investigated MN localization
124 of other importin α subtypes using specific antibodies. IF analyses revealed that importin α3

125 (KPNA4) and importin α5 (KPNA1), which are categorized into subfamilies other than importin
126 α1 (Miyamoto et al., 2016), were also present in MN (Fig. 1E). In addition, importin α3 and
127 importin α5 appeared to colocalize with importin α1 in the same MN (Fig. S3A), indicating that
128 molecular accumulation in the MN is a common feature of the importin α subtypes. We found
129 that when HeLa cells were transfected with enhanced green fluorescence protein (EGFP)-fused
130 importin α1 followed by reversine treatment, the EGFP signals were in some, but not all, MN, as
131 well as in PN (Fig. S3B), confirming the ability of importin α to localize in the MN. Overall, our
132 results reveal a previously unacknowledged feature of importin α family proteins, which are
133 targeted and concentrated in the MN of human cancer-derived cell lines.
134
135 **Association of importin α1 with canonical nuclear transport factors and the nuclear**
136 **envelope in MN**
137 To investigate the concentration of canonical nuclear transport factors within the MN, we
138 examined the localization of importin β1 and CAS/CSE1L, which are known to be associated
139 with importin α, in the Ran GTPase-dependent nuclear transport system. Using IF analysis with
140 antibodies against importin β1, we observed two distinct staining patterns. In the first pattern,
141 importin β1 signals appeared at the rim of the MN, with negligible overlap with importin α1
142 signals in the MN (Fig. 2A upper panels: Cell #1). In the second pattern, both importin α1 and β1
143 signals were detected within MN (Fig. 2A lower panels: Cell #2). Notably, the ratio of MN with
144 importin β1 signals was less than 17% of the total MN, which was considerably lower than the
145 ratio of MN with importin α1 signals (Fig. 2B), and most of the importin β1 signals represented
146 the rim-localized type. In contrast, CAS/CSE1L signals were detected in the majority (up to 88%)
147 of MN in HeLa cells (Fig. 2B,C). These results indicate an inconsistency in the localization of
148 importin α1, importin β1, and CAS/CSE1L within MN, suggesting that the accumulation of

149 importin α1 in MN is regulated independently of the canonical nuclear transport factors.

150 Next, we examined the association between importin α1 and the nuclear envelope (NE)
151 proteins, such as nucleoporins (NUPs) and lamin A/C or lamin B. As MN formation is frequently
152 linked to NE defects that can perturb nuclear trafficking (Guo et al., 2020; Hatch et al., 2013;
153 Maciejowski and Hatch, 2020), we investigated whether MN accumulation of importin α1 was
154 related to NE defects. Using the mAb414 antibody that detects NUPs, we found that the
155 accumulation of importin α1 was not consistently detected in MN associated with NPC deficiency
156 (Fig. 2D); that is, both importin α1-positive MN with NPC signals (yellow arrowhead in Cell #1
157 and #2; upper and lower panels) and importin α1-negative MN with NPC signals (white arrow in
158 Cell #2; lower panel) were detected. Additionally, neither lamin A/C nor lamin B showed a strong
159 correlation with importin α1 localization in MN [Fig. 2E,F; upper panels; i.e., both importin α1-
160 positive MN with lamin signals (yellow arrowhead in Cell #1) and importin α1-negative MN with
161 lamin signals (white arrow in Cell #1)]. However, it should be mentioned that we observed a
162 tendency for importin α1 to be enriched in the lamin-deficient area of MN (Fig. 2E,F; lower panels,
163 Cell #2). These results indicate an inconsistency between NE defects and importin α accumulation
164 in MN, suggesting that NE deficiency is not necessarily involved in importin α enrichment in MN,
165 although a substantial amount of importin α1 accumulation was observed in MN with NE defects.
166

167 **Epigenetic chromatin status and importin α distribution in MN**

168 In a previous study, we demonstrated that importin α is involved in the regulation of gene
169 expression through its association with DNase-sensitive chromatin in response to several stress
170 exposures (Yasuda et al., 2012). Given its role in facilitating the accessibility of nuclear proteins
171 to DNA, we expected importin α to localize predominantly in euchromatin rather than in
172 condensed heterochromatin/silent chromatin regions. To investigate the relationship between

173 importin α1 accumulation and DNA/chromatin status in MN, we performed IF using two different
174 antibodies against histone H3 modifications. One was an antibody against histone H3 modified
175 by tri-methylation at lysine 4 (H3K4me3), which was used as a marker of euchromatin areas, and
176 the other was an antibody against tri-methylation at lysine 9 (H3K9me3), which was used as a
177 marker of heterochromatin regions. We observed positive correlations between signals derived
178 from the H3K4me3 antibody and those derived from the importin α1 antibody in HeLa cells and
179 MDA-MB-231 cells (Fig. 3A,C). In contrast, H3K9me3 antibody signals showed a negative
180 correlation with importin α1 signals, with H3K9me3 signals concentrated in regions where
181 importin α1 signals were reduced (Fig. 3B,D). The regions where importin α1 signals were
182 detected to a lesser extent were frequently associated with the peripheral area of the MN near the
183 NE; DNA/chromatin fibers were generally condensed around these regions due to the
184 spatial/structural constraints of the NE. Taken together, our data suggested a preferential
185 distribution of importin α1 in euchromatic areas rather than in the heterochromatic regions of MN.
186 This finding implied that importin α was involved in regulating DNA/chromatin remodeling
187 activities, such as gene expression and DNA replication/repair, rather than maintaining silenced
188 chromatin in MN.
189
190 **Search for importin α1-interacting proteins in MN**
191 Given that importin α1 was found to be concentrated in euchromatin areas and was expected to
192 be involved in DNA/chromatin remodeling activities, we aimed to identify potential importin α1-
193 interacting partners that may also participate in MN. To achieve this, we first performed rapid
194 immunoprecipitation mass spectrometry of endogenous proteins (RIME) using MCF7 cells, as
195 RIME is a method for the comprehensive identification of molecules with low affinity or
196 molecules that bind transiently in cells (Mohammed et al., 2016). Using two independent samples

197 from MCF7 cells, we identified 106 proteins as importin α1 interactors and obtained a list of 103
198 candidates by removing overlapping proteins (Fig. 4A and Table S1). Gene ontology analysis
199 using the PANTHER Pathways database (Mi et al., 2013; Thomas et al., 2022) revealed that many
200 of these proteins were involved in DNA replication and p53 pathways related to the DNA damage
201 response (Fig. 4B). To narrow down the candidates involved in MN regulation, we further
202 screened the proteins based on their localization using the online database Human Protein Atlas
203 (HPA) (Pontén et al., 2008; Thul et al., 2017). The HPA database provided IF images for each
204 protein and allowed us to examine the localization of 103 candidates in the PN and/or MN. After
205 reviewing the photographic data, we selected eight proteins out of over 60 candidates:
206 CCAR2/DBC1, TOP2B, SUPT16, PARP1, GTF2I, HDAC1, HDAC2, and DNAJB1 as potential
207 interactors that may cooperate with importin α1 for MN regulation (Fig. 4C). Notably, the signals
208 of CCAR2/DBC1, TOP2B, and SUPT16H were highly merged with importin α1 signals in the
209 MN, based on IF analysis (Table S2). Although their MN localization patterns were not fully
210 consistent with importin α1 enrichment, the identification of these potential importin α1-binding
211 proteins provided additional molecular probes for investigating the quality and regulation of MN
212 in cells.
213
214 **Mutually exclusive MN localization of importin α1 and RAD51**
215 We also investigated chromatin regulators associated with DNA replication and the DNA damage
216 response, in addition to the molecules suggested in RIME. Among the proteins tested, we
217 discovered that RAD51, a homologous recombination (HR) repair protein involved in DNA
218 damage response, accumulated in the MN when HeLa cells were exposed to etoposide, a DNA
219 damage inducer (Fig. 5A). Up to 43% of MN exhibited RAD51-positive signals (Fig. 5B). Most
220 RAD51-positive MN displayed low-intensity signals (Fig. 5C, upper panels: Cell #1, white

221 arrowhead), while a small number of MN showed remarkably stronger fluorescence intensity,
222 albeit very rarely (Fig. 5C, lower panels: Cell #2, yellow arrowhead). Interestingly, we found that
223 the localization of importin α1 and RAD51 in the MN was mutually exclusive. The MN with low
224 RAD51 signal intensity exhibited strong importin α1 signal intensity (Fig. 5D, upper panels: Cell
225 #1, yellow arrowhead), whereas MN with strong RAD51 signal intensity showed less importin
226 α1 signal (Fig. 5D, lower panels: Cell #2, white arrowhead). Furthermore, we observed the
227 compartmentalization of these molecules in MN within a single cell (Fig. 5E, Cells #1 and #2:
228 yellow arrowhead; importin α1-positive and RAD51-negative MN; white arrowhead; importin
229 α1-negative and RAD51-positive MN). This observation suggested that RAD51, in contrast to
230 importin α1, served as another probe characterizing the microenvironment of MN.
231
232 **Possible mechanism for RAD51 exclusion from importin α1-enriched MN**
233 We investigated the mechanisms underlying the exclusion of RAD51 from importin α1-enriched
234 MN. To examine the effect of protein expression on subcellular localization, we co-overexpressed
235 mCherry-RAD51 and EGFP-importin α1 in HeLa cells. Intriguingly, cells overexpressing EGFP-
236 importin α1 showed the altered nuclear distribution of mCherry-RAD51 to the cytoplasm,
237 implying a mutual exclusion effect between the two proteins (Fig. S4A,B). We also observed a
238 similar effect on RAD51 localization when FLAG-importin α1 was expressed at high levels and
239 localized to the nucleus (Fig. S4C, upper panel; Cell #1). In contrast, when FLAG-importin α1
240 was expressed at low levels and localized in the cytoplasm, mCherry-RAD51 remained
241 exclusively in the nucleus (Fig. S4C; lower panel; Cell #2). Additionally, we investigated whether
242 endogenous RAD51 was diminished in cells overexpressing EGFP-importin α1 and then clarified
243 the mutual exclusion effect (Fig. S4D,E). Based on these observations, we proposed that the
244 subcellular localization of RAD51 was influenced by the relative expression levels and/or

concentrations of importin α1 within the limited area in cells. Finally, we examined the applicability of the mutual exclusion mechanism of importin α1 and RAD51 in the MN microenvironment. IF analysis revealed a marked reduction in endogenous RAD51 signals in the MN of cells overexpressing EGFP-importin α1 (Fig. 5F,G), supporting the mutual exclusion of importin α1 and RAD51 in MN.

251 **DISCUSSION**

252 The molecular mechanisms underlying the emergence, quality, and fate of MN remain largely
253 unknown. In this study, we found that the importin αs, particularly importin α1 (KPNA2), were
254 expressed at higher levels in the human cancer cell lines tested. Moreover, we demonstrated that
255 importin α1 was enriched in up to 40% of the MN generated in HeLa cells. Remarkably, a similar
256 phenomenon was observed in other human cancer cell lines, such as MCF7 and MDA-MB-231,
257 suggesting that importin α1 accumulation in MN was a common feature of multiple cultured
258 cancer cells. Furthermore, we observed the presence of other importin α subtypes, importin α3
259 and importin α5, in the MN, which overlapped with importin α1 in the same MN. These findings
260 revealed a previously unrecognized feature of the importin α family proteins, indicating their role
261 in controlling MN structure and function.

262 It is intriguing that importin α localizes to some but not all MN. The precise targeting
263 mechanism responsible for the localization of importin α to a subset of MN, as well as its
264 implication for the quality and outcome of MN, remains unanswered. In this study, we examined
265 the cellular distribution of canonical nuclear transport factors, such as importin β1 and
266 CAS/CSE1L, along with NE protein deficiency. However, these factors did not fully align with
267 the behavior of importin α accumulation in MN. This suggested that the localization of importin
268 α to MN was regulated independently of the Ran-dependent nuclear transport machinery and was
269 not solely a consequence of NE defects in MN. Notably, importin α has been reported to have
270 non-transport functions during mitotic spindle formation and/or microtubule nucleation (Gruss et
271 al., 2001; Schatz et al., 2003). Importin α binds to spindle assembly factors (SAFs), such as TPX2
272 and NuMA, and inhibits the accessibility of SAFs to microtubules, thereby controlling the higher-
273 order assembly of microtubules (Chang and Hsia, 2021; Forbes et al., 2015). Considering that
274 MN formation resulted from asymmetric chromosome segregation caused by mitotic errors

275 during cell division, which leads to lagging chromosomes and chromosome fragments (Kwon et
276 al., 2020; Terradas et al., 2016), it is plausible that the aberrant dissociation of SAFs from importin
277 α during mitosis could result in chromosome lagging or fragmentation. This, in turn, may affect
278 MN formation and ultimately lead to importin α accumulation in the MN, independent of the
279 canonical nuclear transport function. Further investigations are required to comprehensively
280 understand the mechanism by which importin α targets MN.

281 Our data on the distribution of importin α1 and histone modification markers revealed that
282 importin α1 distribution coincided with H3K4me3-rich chromatin regions in MN. However, the
283 mechanism by which importin α1 recognizes and is maintained in open chromatin remains unclear.
284 In a previous study, we demonstrated that nuclear-localized importin α could associate with
285 DNase-sensitive chromatin components and become involved in gene regulation (Yasuda et al.,
286 2012). Additionally, another group reported the DNA-binding property of importin α (Jibiki et al.,
287 2021). Based on these findings, we hypothesized that the ability of importin α to associate with
288 DNA/chromatin fibers may be attributed to its intrinsic DNA/chromatin binding capacity. This
289 suggests that importin α may contribute to the establishment and/or maintenance of open
290 chromatin in MN, potentially through the cooperation of importin α with other chromatin
291 regulators such as gene expression/silencing factors and DNA replication/repair proteins. It was
292 interesting to speculate that the eight proteins identified as importin α1-binding partners through
293 RIME analysis were suitable candidates for consideration as such collaborators. Specifically, our
294 interest lay in CCAR2/DBC1, TOP2B, and SUPT16H as importin α-collaborators, with an
295 overlapped ratio of 95%, 93%, and 92% respectively, with the importin α1 signals (Table S2).
296 CCAR2/DBC1 regulates cell survival and death in response to genotoxic and metabolic stresses
297 (Magni et al., 2015). TOP2B is a well-known enzyme that decoils chromatin and releases torsional
298 force into the DNA (Gonzalez-Buendia et al., 2021). Its association with chromatin sites marked

299 by H3K4me3 (Tiwari et al., 2012) and MN (Muciño-Hernández et al., 2023) has also been
300 reported. SUPT16H is a component of the facilitates chromatin transcription (FACT) complex,
301 involved in multiple processes such as mRNA elongation, DNA replication, and DNA damage
302 repair (Oliveira et al., 2014). Considering the importance of these proteins in DNA/chromatin
303 quality control, we are currently investigating the biological consequences of their interaction
304 with importin α on DNA/chromatin fibers in the MN microenvironment.

305 The role of importin α in the outcome of MN remains unclear. We provided evidence
306 for the molecular connection between importin α1 and RAD51, which revealed a novel function
307 of importin α1 in regulating the subcellular localization of RAD51 when importin α1 is highly
308 expressed. Although RAD51 was not initially identified as a binding partner in RIME analysis, a
309 previous study identified importin α1 (described as importin α2) as a component of the RAD51
310 complex with CAS/CSE1L (Okimoto et al., 2015), suggesting an interrelationship between
311 importin α1 and RAD51, particularly in subcellular distribution. RAD51 plays a crucial role in
312 DNA repair via homologous recombination, which is vital for maintaining genomic stability and
313 preventing mutation accumulation (Wassing and Esashi, 2021). Increased RAD51 expression
314 promotes recombination events and genome instability in tumor cells (Klein, 2008; Richardson
315 et al., 2004). Importantly, both importin α1 and RAD51 have been implicated in tumorigenesis
316 and patient survival (Christiansen and Dyrskjot, 2013; Han and Wang, 2020; Liao et al., 2022).
317 Therefore, the enrichment of importin α1 in MN, along with its interaction with DNA/chromatin,
318 may constitute a system that safeguards the genome from RAD51 activity. This notion was
319 supported by the observation that breast cancer tissues with high expression of importin α1 exhibit
320 the cytoplasmic localization of RAD51 (Alshareeda et al., 2015). Further investigations into the
321 subcellular distribution dynamics of importin α1 and RAD51 are imperative for comprehending
322 cancer progression and malignancy.

323 Although the mechanism by which importin α targets MN and interacts with
324 DNA/chromatin regulators in MN while excluding RAD51 from MN remains unclear, our results
325 demonstrate that importin α served as a previously undescribed molecular marker that can be used
326 to characterize the MN microenvironment. These findings will be beneficial for researchers
327 interested in studying the heterogeneity, quality control, and fate of MN in cancer cells.
328

329 **MATERIALS AND METHODS**

330 **Cell lines and culture conditions**

331 Human cervical cancer cell line HeLa cells were obtained from the RIKEN cell bank (Tsukuba,
332 Japan). Human breast cancer cell line MCF7 was obtained from NIBIOHN (JCRB 0134), and
333 MDA-MB-231, SK-BR-3, and human breast epithelial cell line MCF10A were kindly gifted from
334 Satoshi Fujii (National Cancer Center, Japan). HeLa cells were maintained in Dulbecco's
335 modified Eagle's medium (D-MEM) /Ham's F-12 nutrient mixture containing 5% fetal bovine
336 serum (FBS). MCF7 cells were maintained in Minimum Essential Medium (MEM) Alpha no
337 phenol red (Life Technologies, Carlsbad, CA) containing 10 % FBS, 0.1 mM MEM Non-essential
338 amino acids (NEAA; Life Technologies), 1 mM Sodium pyruvate (Life Technologies), and 10
339 μg/mL Insulin (Wako, Osaka, Japan). MDA-MB-231 cells were cultured in the RPMI1640
340 medium (Sigma-Aldrich, St. Louis, MO, USA) containing 10 % FBS and 2 mM L-Glutamine
341 (Life Technologies). SK-BR-3 cells were maintained in DMEM with 10 % FBS. MCF10A cells
342 were cultured in MEG mammary epithelial cell growth medium BulletKit added to SingleQuote
343 (CC-3150) and 10 % FBS. Cells were cultured at 37 °C in a 5% CO2 incubator. Reversine
344 (Cayman Chemical, MI, USA) and etoposide (Tokyo Chemical Industry (TCI) Co., LTD., Tokyo,
345 Japan) were used as described in Fig. S2 and Fig. 5.

346

347 **Animal care and use**

348 Experimental procedures in production of monoclonal antibodies were approved by the CEC
349 Animal Care and Use Committee and performed according to CEC Animal Experimentation
350 Regulations.

351

352 **Antibodies**

353 Primary antibodies used in the experiments are listed in Table S3. A new mouse monoclonal
354 antibody that specifically recognized the importin α6 (KPNA5) protein was generated and named
355 Clone number 1E3-2D6. As an antigen for immunization, the bacterially-produced recombinant
356 importin α6 was purified as described previously (Miyamoto and Oka, 2016). An 8-week-old
357 female C57BL/6 mouse (SLC, Shizuoka, Japan) was injected into the tail base with 100 μL of
358 emulsions containing the recombinant importin α6 protein and Freund's complete adjuvant.
359 Briefly, 17 days after the first immunization, an additional immunization of the importin α6 protein
360 was performed without an adjuvant into the tail base of the mouse. Four days after the additional
361 immunization, cells from the iliac lymph nodes of the immunized mouse were fused with mouse
362 myeloma Sp2/0-Ag14 cells at a ratio of 5:1 in 50% polyethylene glycol. The resulting hybridoma
363 cells were plated onto 96-well plates and cultured in a HAT selection medium. The importin α6-
364 specific antibody was screened by ELISA, western blotting, and immunostaining using hybridoma
365 supernatants. Finally, a hybridoma clone-producing monoclonal antibody named 1E3-2D6 was
366 selected. The Mab 1E3-2D6 was found to be an IgG 2a (k) subtype using a mouse isotyping kit.
367 The secondary antibodies used were: Alexa Fluor Plus 488 (A32723, A32790, A32731, and
368 A32814; Thermo Fisher Scientific Inc, Rockford, IL, USA), and Alexa Fluor 488 (A11055), Alexa
369 Fluor 594 (A-21203, A32754, and A11032) for an indirect immunofluorescence and horseradish
370 peroxidase (HRP)-conjugated anti-goat, anti-rabbit, or anti-mouse secondary antibodies (Jackson
371 ImmunoResearch Inc West Grove, PA, USA) for western blotting.
372

373 **Immunofluorescence analysis**

374 MCF7, MDA-MB-231, and HeLa cell lines were cultured on 18 × 18 mm coverslips (Menzel-
375 Glaser, Braunschweig, Germany) in a 35 mm dish, and immunofluorescence analysis was
376 performed as follows. Cells were fixed with 3.7% formaldehyde in phosphate-buffered saline

377 (PBS) for 15 min, followed by treatment with 0.5% Triton X-100 in PBS for 5 min. After blocking
378 with 3% skim milk in PBS for 30 min at 25°C, the cells on the coverslips were labeled with
379 primary antibodies overnight and following by reacted with secondary antibodies accordingly for
380 1 h at 25°C. To visualize DNA, the slides were incubated with DAPI (1:5000 in PBS, Dojindo)
381 for 20 min. The fluorescence images were observed using a confocal microscope (Leica TCS SP8
382 II; Leica Microsystems, Wetzlar, Germany).
383
384 **Plasmid construction for mammalian expression**
385 Human importin α1 (KPNA2) cDNA subcloned into the pGEX6P2 plasmid was gifted from Akira
386 Tsujii (NIBIOHN) and then cloned into pEGFPC1 vector (Clontech, Mountain View, CA, USA).
387 pEGFPC1-mouse importin α2 (KPNA2) was constructed as described previously (Yasuda et al.,
388 2012). The pcDNA5/FRT/3xFLAG-importin α1 (KPNA2) was constructed as previously
389 described (Kimoto et al., 2015). The cDNA encoding RAD51 was amplified from HeLa cells by
390 PCR using the following primers: forward: 5'-
391 GTCCGGACTCAGATCTATGGCAATGCAGATGCAGCT-3' and reverse: 5'-
392 CCGCGGTACCGTCGACTCAGTCTTTGGCATCTCCCACT-3'. The cDNAs were cloned into
393 the pmCherryC1 vector using an In-Fusion HD cloning kit (Clontech, Mountain View, CA, USA).
394
395 **Transfection and siRNAs**
396 HeLa cells were plated onto 18 × 18 mm coverslips (Menzel-Glaser) in a 35-mm dish 2 days prior
397 to transfection. The transfections for mammalian expression plasmids were performed using
398 Lipofectamine 2000 DNA Transfection Reagent (Thermo Fisher Scientific) following the
399 manufacturer's instructions.
400

401 **Western blotting**

402 Western blotting was performed as previously described (Miyamoto et al., 2022). The membranes
403 were incubated with primary antibodies (dilutions ranging from 1:2000) diluted in Can Get Signal
404 Immunoreaction Enhancer Solution 1 (TOYOBO, Osaka, Japan) overnight at 4 °C. The used
405 HRP-conjugated secondary antibodies (dilutions ranging from 1:8000 to 1:10,000) were diluted
406 in Can Get Signal Immunoreaction Enhancer Solution 2 (TOYOBO) at 25 °C for 1 h. The signals
407 were detected with ATTO EzWest lumi plus (WSE-7120S, ATTO Corporation, Tokyo, Japan).

408

409 **Rapid immunoprecipitation mass spectrometry of endogenous proteins (RIME)**

410 MCF-7 cells (1.5 x 10^6) were cultured in 100-mm dishes (IWAKI, Tokyo, Japan) in 10 mL of
411 MEM medium with 10% FBS for 5 days. To fix the cells, 1/10 volume (1 mL) of freshly prepared
412 Formaldehyde Solutions [FS: 11% Methanol free formaldehyde, 0.1 M NaCl, 1 mM EDTA, and
413 50 mM Hepes (pH7.9)] was directly added to the medium and incubated for 8 min at 25°C. After
414 the addition of 0.55 mL 2.5 M glycine solution to the 11 mL of the medium (final conc. 0.1 M)
415 to quench crosslinking for 5 min, cells were washed twice with ice-cold phosphate-buffered saline
416 (PBS). After removal of the supernatants, cells were collected at 800 x *g* for 10 min at 4°C, and
417 then, the cell pellets were resuspended with 10 mL of ice-cold PBS with 0.5% Igepal CA-630 (#I-
418 8896, Sigma-Aldrich) and then centrifuged again. The cell pellets were suspended with 10 mL of
419 ice-cold PBS with 0.5% Igepal CA-630 and 100 μL of 100 mM PMSF in EtOH (final conc. 1
420 mM). The cell suspension was centrifuged thrice to pellet the cells, and then, the cell pellets were
421 snap-frozen in liquid N2 and stored at -80 °C. RIME analysis was performed by Active Motif,
422 CA., according to published protocols (Mohammed et al., 2016). RIME was carried out using an
423 antibody against KPNA2 (Abcam, Cat. # ab84440, Table S3) and 150 μg of chromatin from
424 MCF7 cells to identify proteins that interact with KPNA2 using mass spectrometry. Mass

425 spectrometry of the immunoprecipitated protein complexes resulted in 57–60% coverage of
426 importin α1.
427
428 **Statistical analysis**
429 Cells and MN were counted optically under a microscope using the appropriate fluorescence field.
430 Unless stated otherwise, all data are presented as the mean ± standard deviation (s.d.). Within
431 individual experiments, data points were based on a minimum of triplicate representative samples.
432 Data were analyzed with Prism 9.0 software (GraphPad Software, La Jolla, CA).

Acknowledgments

We thank Akira Tsujii (NIBIOHN) for kindly gifting the pGEX6P2-human importin α1 plasmid and Satoshi Fujii (National Cancer Center, Japan) for kindly gifting the human breast epithelial cells. We also thank all the members of the Oka and the Saitoh Laboratory for their helpful discussion and technical support.

Funding

This work was supported by Japan Society for the Promotion of Science (JSPS) KAKENHI grant numbers JP20K06455 and JP22KK0111 to Y.M., JP17H01878 to H.S., and The Naito Foundation (Japan) to H.S.

Competing interests

No competing interests declared.

Author contributions

YM and HS conceived originally the project. YM, RK, MO, and HS designed the project and experiments. YM, RK, RO, CH, and TT performed the experiments. YM, RK, and HS analyzed the data and designed figures. YM and HS wrote the manuscript.

451 **REFERENCES**

452 **Alshareeda, A. T., Negm, O. H., Green, A. R., Nolan, C. C., Tighe, P., Albarakati, N., Sultana,**
453 **R., Madhusudan, S., Ellis, I. O. and Rakha, E. A.** (2015). KPNA2 is a nuclear export
454 protein that contributes to aberrant localisation of key proteins and poor prognosis of
455 breast cancer. *Br J Cancer* **112**, 1929-1937.

456 **Behrens, P., Brinkmann, U. and Wellmann, A.** (2003). CSE1L/CAS: its role in proliferation
457 and apoptosis. *Apoptosis* **8**, 39-44.

458 **Chang, C. C. and Hsia, K. C.** (2021). More than a zip code: global modulation of cellular
459 function by nuclear localization signals. *FEBS J* **288**, 5569-5585.

460 **Christiansen, A. and Dyrskjot, L.** (2013). The functional role of the novel biomarker
461 karyopherin α2 (KPNA2) in cancer. *Cancer Lett* **331**, 18-23.

462 **Dahl, E., Kristiansen, G., Gottlob, K., Klaman, I., Ebner, E., Hinzmann, B., Hermann, K.,**
463 **Pilarsky, C., Durst, M., Klinkhammer-Schalke, M., et al.** (2006). Molecular profiling
464 of laser-microdissected matched tumor and normal breast tissue identifies karyopherin
465 alpha2 as a potential novel prognostic marker in breast cancer. *Clin Cancer Res* **12**, 3950-
466 3960.

467 **Dankof, A., Fritzsche, F. R., Dahl, E., Pahl, S., Wild, P., Dietel, M., Hartmann, A. and**
468 **Kristiansen, G.** (2007). KPNA2 protein expression in invasive breast carcinoma and
469 matched peritumoral ductal carcinoma in situ. *Virchows Arch* **451**, 877-881.

470 **Forbes, D. J., Travesa, A., Nord, M. S. and Bernis, C.** (2015). Nuclear transport factors: global
471 regulation of mitosis. *Curr Opin Cell Biol* **35**, 78-90.

472 **Forment, J. V., Kaidi, A. and Jackson, S. P.** (2012). Chromothripsis and cancer: causes and
473 consequences of chromosome shattering. *Nat Rev Cancer* **12**, 663-670.

474 **Furuta, M., Kose, S., Koike, M., Shimi, T., Hiraoka, Y., Yoneda, Y., Haraguchi, T. and**
475 **Imamoto, N.** (2004). Heat-shock induced nuclear retention and recycling inhibition of
476 importin α. *Genes Cells* **9**, 429-441.

477 **Goldfarb, D. S., Corbett, A. H., Mason, D. A., Harreman, M. T. and Adam, S. A.** (2004).
478 Importin α: a multipurpose nuclear-transport receptor. *Trends Cell Biol* **14**, 505-514.

479 **Gonzalez-Buendia, E., Zhao, J., Wang, L., Mukherjee, S., Zhang, D., Arrieta, V. A., Feldstein,**
480 **E., Kane, J. R., Kang, S. J., Lee-Chang, C., et al.** (2021). TOP2B Enzymatic Activity
481 on Promoters and Introns Modulates Multiple Oncogenes in Human Gliomas. *Clin*
482 *Cancer Res* **27**, 5669-5680.

483 **Gruss, O. J., Carazo-Salas, R. E., Schatz, C. A., Guarguaglini, G., Kast, J., Wilm, M., Le**
484 **Bot, N., Vernos, I., Karsenti, E. and Mattaj, I. W.** (2001). Ran induces spindle assembly
485 by reversing the inhibitory effect of importin α on TPX2 activity. *Cell* **104**, 83-93.

486 **Guo, X., Dai, X., Wu, X., Zhou, T., Ni, J., Xue, J. and Wang, X.** (2020). Understanding the

487 birth of rupture-prone and irreparable micronuclei. *Chromosoma* **129**, 181-200.
488 **Han, Y. and Wang, X.** (2020). The emerging roles of KPNA2 in cancer. *Life Sci* **241**, 117140.
489 **Hatch, E. M., Fischer, A. H., Deerinck, T. J. and Hetzer, M. W.** (2013). Catastrophic nuclear
490 envelope collapse in cancer cell micronuclei. *Cell* **154**, 47-60.
491 **Hintzsche, H., Hemmann, U., Poth, A., Utesch, D., Lott, J. and Stopper, H.** (2017). Fate of
492 micronuclei and micronucleated cells. *Mutat Res Rev Mutat Res* **771**, 85-98.
493 **Jibiki, K., Kodama, T. S., Suenaga, A., Kawase, Y., Shibazaki, N., Nomoto, S., Nagasawa, S.,**
494 **Nagashima, M., Shimodan, S., Kikuchi, R., et al.** (2021). Importin α2 association with
495 chromatin: Direct DNA binding via a novel DNA-binding domain. *Genes Cells* **26**, 945-
496 966.
497 **Kimoto, C., Moriyama, T., Tsujii, A., Igarashi, Y., Obuse, C., Miyamoto, Y., Oka, M. and**
498 **Yoneda, Y.** (2015). Functional characterization of importin α8 as a classical nuclear
499 localization signal receptor. *Biochim Biophys Acta* **1853**, 2676-2683.
500 **Klein, H. L.** (2008). The consequences of Rad51 overexpression for normal and tumor cells. *DNA*
501 *Repair (Amst)* **7**, 686-693.
502 **Kodiha, M., Banski, P., Ho-Wo-Cheong, D. and Stochaj, U.** (2008). Dissection of the molecular
503 mechanisms that control the nuclear accumulation of transport factors importin-α and
504 CAS in stressed cells. *Cell Mol Life Sci* **65**, 1756-1767.
505 **Krupina, K., Goginashvili, A. and Cleveland, D. W.** (2021). Causes and consequences of
506 micronuclei. *Curr Opin Cell Biol* **70**, 91-99.
507 **Kwon, M., Leibowitz, M. L. and Lee, J. H.** (2020). Small but mighty: the causes and
508 consequences of micronucleus rupture. *Exp Mol Med* **52**, 1777-1786.
509 **Liao, C., Talluri, S., Zhao, J., Mu, S., Kumar, S., Shi, J., Buon, L., Munshi, N. C. and**
510 **Shammas, M. A.** (2022). RAD51 Is Implicated in DNA Damage, Chemoresistance and
511 Immune Dysregulation in Solid Tumors. *Cancers (Basel)* **14**.
512 **Liu, J. and Hetzer, M. W.** (2022). Nuclear pore complex maintenance and implications for age-
513 related diseases. *Trends Cell Biol* **32**, 216-227.
514 **Ly, P. and Cleveland, D. W.** (2017). Rebuilding Chromosomes After Catastrophe: Emerging
515 Mechanisms of Chromothripsis. *Trends Cell Biol* **27**, 917-930.
516 **Maciejowski, J. and Hatch, E. M.** (2020). Nuclear Membrane Rupture and Its Consequences.
517 *Annu Rev Cell Dev Biol* **36**, 85-114.
518 **Magni, M., Ruscica, V., Restelli, M., Fontanella, E., Buscemi, G. and Zannini, L.** (2015).
519 CCAR2/DBC1 is required for Chk2-dependent KAP1 phosphorylation and repair of
520 DNA damage. *Oncotarget* **6**, 17817-17831.
521 **Mi, H., Muruganujan, A. and Thomas, P. D.** (2013). PANTHER in 2013: modeling the
522 evolution of gene function, and other gene attributes, in the context of phylogenetic trees.

Nucleic Acids Res **41**, D377-386.

Miller, K. N., Victorelli, S. G., Salmonowicz, H., Dasgupta, N., Liu, T., Passos, J. F. and Adams, P. D. (2021). Cytoplasmic DNA: sources, sensing, and role in aging and disease. *Cell* **184**, 5506-5526.

Miyamoto, Y., Itoh, Y., Suzuki, T., Tanaka, T., Sakai, Y., Koido, M., Hata, C., Wang, C. X., Otani, M., Moriishi, K., et al. (2022). SARS-CoV-2 ORF6 disrupts nucleocytoplasmic trafficking to advance viral replication. *Commun Biol* **5**, 483.

Miyamoto, Y. and Oka, M. (2016). Data on dimer formation between importin α subtypes. *Data Brief.* **7**, 1248-1253

Miyamoto, Y., Saiwaki, T., Yamashita, J., Yasuda, Y., Kotera, I., Shibata, S., Shigeta, M., Hiraoka, Y., Haraguchi, T. and Yoneda, Y. (2004). Cellular stresses induce the nuclear accumulation of importin α and cause a conventional nuclear import block. *J Cell Biol* **165**, 617-623.

Miyamoto, Y., Yamada, K. and Yoneda, Y. (2016). Importin α: a key molecule in nuclear transport and non-transport functions. *J Biochem* **160**, 69-75.

Miyazaki, K., Ichikawa, Y., Saitoh, N. and Saitoh, H. (2020). Three Types of Nuclear Envelope Assemblies Associated with Micronuclei. *CellBio* **9**, 14-28.

Mohammed, H., Taylor, C., Brown, G. D., Papachristou, E. K., Carroll, J. S. and D'Santos, C. S. (2016). Rapid immunoprecipitation mass spectrometry of endogenous proteins (RIME) for analysis of chromatin complexes. *Nat Protoc* **11**, 316-326.

Muciño-Hernández, G., Acevo-Rodríguez, P. S., Cabrera-Benitez, S., Guerrero, A. O., Merchant-Larios, H. and Castro-Obregón, S. (2023). Nucleophagy contributes to genome stability through degradation of type II topoisomerases A and B and nucleolar components. *J Cell Sci* **136**.

Oka, M. and Yoneda, Y. (2018). Importin α: functions as a nuclear transport factor and beyond. *Proc Jpn Acad Ser B Phys Biol Sci* **94**, 259-274.

Okimoto, S., Sun, J., Fukuto, A., Horikoshi, Y., Matsuda, S., Matsuda, T., Ikura, M., Ikura, T., Machida, S., Kurumizaka, H., et al. (2015). hCAS/CSE1L regulates RAD51 distribution and focus formation for homologous recombinational repair. *Genes Cells* **20**, 681-694.

Oliveira, D. V., Kato, A., Nakamura, K., Ikura, T., Okada, M., Kobayashi, J., Yanagihara, H., Saito, Y., Tauchi, H. and Komatsu, K. (2014). Histone chaperone FACT regulates homologous recombination by chromatin remodeling through interaction with RNF20. *J Cell Sci* **127**, 763-772.

Pontén, F., Jirström, K. and Uhlen, M. (2008). The Human Protein Atlas--a tool for pathology. *J Pathol* **216**, 387-393.

559 **Poon, I. K. and Jans, D. A.** (2005). Regulation of nuclear transport: central role in development
560 and transformation? *Traffic* **6**, 173-186.
561 **Pumroy, R. A. and Cingolani, G.** (2015). Diversification of importin-α isoforms in cellular
562 trafficking and disease states. *Biochem J* **466**, 13-28.
563 **Richardson, C., Stark, J. M., Ommundsen, M. and Jasin, M.** (2004). Rad51 overexpression
564 promotes alternative double-strand break repair pathways and genome instability.
565 *Oncogene* **23**, 546-553.
566 **Schatz, C. A., Santarella, R., Hoenger, A., Karsenti, E., Mattaj, I. W., Gruss, O. J. and**
567 **Carazo-Salas, R. E.** (2003). Importin alpha-regulated nucleation of microtubules by
568 TPX2. *Embo J* **22**, 2060-2070.
569 **Stelma, T., Chi, A., van der Watt, P. J., Verrico, A., Lavia, P. and Leaner, V. D.** (2016).
570 Targeting nuclear transporters in cancer: Diagnostic, prognostic and therapeutic potential.
571 *IUBMB Life* **68**, 268-280.
572 **Stewart, M.** (2007). Molecular mechanism of the nuclear protein import cycle. *Nat Rev Mol Cell*
573 *Biol* **8**, 195-208.
574 **Storchová, Z. and Kloosterman, W. P.** (2016). The genomic characteristics and cellular origin
575 of chromothripsis. *Curr Opin Cell Biol* **40**, 106-113.
576 **Sun, Y., Li, W., Li, X., Zheng, H., Qiu, Y. and Yang, H.** (2021). Oncogenic role of karyopherin
577 α2 (KPNA2) in human tumors: A pan-cancer analysis. *Comput Biol Med* **139**, 104955.
578 **Terradas, M., Martín, M. and Genescà, A.** (2016). Impaired nuclear functions in micronuclei
579 results in genome instability and chromothripsis. *Arch Toxicol* **90**, 2657-2667.
580 **Thomas, P. D., Ebert, D., Muruganujan, A., Mushayahama, T., Albou, L. P. and Mi, H.**
581 (2022). PANTHER: Making genome-scale phylogenetics accessible to all. *Protein Sci* **31**,
582 8-22.
583 **Thul, P. J., Åkesson, L., Wiking, M., Mahdessian, D., Geladaki, A., Ait Blal, H., Alm, T.,**
584 **Asplund, A., Björk, L., Breckels, L. M., et al.** (2017). A subcellular map of the human
585 proteome. *Science* **356**.
586 **Tiwari, V. K., Burger, L., Nikoletopoulou, V., Deogracias, R., Thakurela, S., Wirbelauer, C.,**
587 **Kaut, J., Terranova, R., Hoerner, L., Mielke, C., et al.** (2012). Target genes of
588 Topoisomerase IIβ regulate neuronal survival and are defined by their chromatin state.
589 *Proc Natl Acad Sci U S A* **109**, E934-943.
590 **Walde, S. and Kehlenbach, R. H.** (2010). The Part and the Whole: functions of nucleoporins in
591 nucleocytoplasmic transport. *Trends Cell Biol* **20**, 461-469.
592 **Wang, C. I., Chien, K. Y., Wang, C. L., Liu, H. P., Cheng, C. C., Chang, Y. S., Yu, J. S. and**
593 **Yu, C. J.** (2012). Quantitative proteomics reveals regulation of karyopherin subunit
594 alpha-2 (KPNA2) and its potential novel cargo proteins in nonsmall cell lung cancer. *Mol*

Cell Proteomics **11**, 1105-1122.

Wassing, I. E. and Esashi, F. (2021). RAD51: Beyond the break. *Semin Cell Dev Biol* **113**, 38-46.

Wente, S. R. and Rout, M. P. (2010). The nuclear pore complex and nuclear transport. *Cold Spring Harb Perspect Biol* **2**, a000562.

Yasuda, Y., Miyamoto, Y., Yamashiro, T., Asally, M., Masui, A., Wong, C., Loveland, K. L. and Yoneda, Y. (2012). Nuclear retention of importin α coordinates cell fate through changes in gene expression. *EMBO J* **31**, 83-94.

Zhang, C. Z., Spektor, A., Cornils, H., Francis, J. M., Jackson, E. K., Liu, S., Meyerson, M. and Pellman, D. (2015). Chromothripsis from DNA damage in micronuclei. *Nature* **522**, 179-184.

607 **FIGURE LEGENDS**

608 **Fig. 1. Accumulation of importin α proteins in MN.** (A) Exponentially growing MCF7 (upper
609 panels) and HeLa (lower panels) cells are subjected to indirect IF analysis using an anti-importin
610 α1 antibody (Imp-α1, left columns). White dotted lines indicate cellular boundaries. DNA is
611 stained with DAPI (middle columns). Merged images are shown on the right. Bar = 20 μm. The
612 yellow line described with X and Y is for fluorescence analysis in B. (B) Fluorescent intensities
613 of importin α1 (green) and DAPI (blue) are measured along with the X-Y line in the lower right
614 panel (HeLa cells) represented in A. PN: primary nuclei, MN: micronuclei. (C) HeLa cells are
615 subjected to IF using an anti-importin α1 antibody. The pattern of the signals is categorized into
616 three groups: MN with high intensity (yellow arrowhead), low intensity (white arrowhead), or no
617 intensity (white arrow). Bar = 20 μm. (D) The ratio of the importin α1 localized-MN against the
618 whole number of MN in HeLa cells which are treated with 400 nM reversine for 20 h. The number
619 of DAPI-stained MN is counted and the ratio of the importin α1 positive MN is calculated (150
620 cells in total). Ten to fifteen cells per an observed area are counted to derive the percentage of
621 importin α1 positive MN for eight different areas. The graph represents the category of the MN
622 types exhibited in C. "All" (blue), "High" (red), and "Low" (green) mean either all numbers of
623 MN with importin α1 signals, MN with the high signal intensity of importin α1, or MN with the
624 low signal intensity of importin α1, respectively. (E) MCF7 cells are subjected to IF analysis using
625 anti-importin α3 (upper panels) and anti-importin α5 antibodies (lower panels). The yellow
626 arrowheads, white arrowheads, and white arrows indicate MN with either high, low or no intensity
627 of importin αs, respectively. Bar = 20 μm.

628

629 **Fig. 2. Localization of importin β1, CAS/CSE1L, and nuclear membrane proteins in**
630 **importin α1-enriched MN.**

631 (A) IF analysis of importin α1 and importin β1 in reversine-treated HeLa cells. Two images of
632 independent cells are shown in the upper (Cell #1) and lower panels (Cell #2). DNA is stained
633 with DAPI. Merged images are shown on the right side. White dotted lines indicate cellular
634 boundaries. Yellow arrowhead: high intensity of importin α1 signals. Bar = 10 μm. (B) Ratio of
635 importin β1- or CAS/CSE1L-localized-MN against the total number of MN in reversine-treated
636 HeLa cells. The number of DAPI-stained MN (100 cells in total) is counted for independent
637 experiments (n=4) and the ratio of importin β1- or CAS/CSE1L-positive MN is calculated. (C)
638 MN localization of importin α1 and CAS/CSE1L in the reversine-treated HeLa cells. Yellow
639 arrowhead: high intensity of importin α1 signals, white arrowhead: low intensity of importin α1
640 signals. Bar = 10 μm. (D–F) IF analysis for importin α1 and either nucleoporin (D, is shown as
641 NPC), Lamin A/C (E), or Lamin B1 (F) in reversine-treated HeLa cells. Yellow arrowhead, high
642 intensity of importin α1 signals; white arrow, no importin α1 signals. Bar = 10 μm. (E,F) Two
643 images of an independent cell are shown in the upper panel (Cell #1), and the lower panels show
644 an enlarged MN image (Cell #2). The fluorescence intensities of importin α1 (green), Lamin A/C
645 or Lamin B1 (red), and DAPI (blue) are measured along with the X-Y line in the lower panel (Cell
646 #2).
647
648 **Fig. 3. Co-localization of importin α1 signals with H3K4me3 signals in MN.**
649 (A–D) MN localization of importin α1 with H3K4me3 (A,C) or H3K9me3 (B,D) in reversine
650 treated HeLa cells (A,B) or normally cultured MDA-MB-231 (C,D). The upper enlarged images
651 are extracted from the area enclosed by the red dotted line in the lower image. DNA is stained
652 with DAPI, and merged images are shown on the right side. Fluorescent intensities of importin
653 α1 (green), modified histones (red: H3K4me3 or H3K9me3), and DAPI (blue) in MN are
654 measured along with the X-Y line and represented in the left low. Bar = 10 μm.

655

656 **Fig. 4. Exploration of importin α1-binding proteins through the RIME analysis.**

657 (A) Venn diagram grouping candidate importin α1-binding proteins by RIME. Two independent
658 experiments are performed. MCF7-R1 and MCF7-R2 are proteins precipitated by anti-importin
659 α1 antibodies, and IgG Control-R1 and -R2 are proteins precipitated by normal IgG antibodies.
660 One hundred and six proteins are candidate binding partners of importin α1. (B) Gene Ontology
661 analysis for identified binding proteins. All gene ontology terms are identified as a result of
662 querying the PANTHER Pathways database for the importin α1-interacting proteins identified by
663 RIME. Terms are ranked by p-value. (C) IF analysis for MN localization of importin α1 and
664 candidate molecules identified by RIME in HeLa cells. Cells are treated with 400 nM reversine
665 for 20 h, and then, the molecules described are detected by the specific antibodies. White dotted
666 lines indicate cellular boundaries. DNA is stained with DAPI. Merged images are shown on the
667 right side. The yellow arrowheads, white arrowheads, and white arrows indicate MN with either
668 high intensity, low intensity, or no intensity of importin αs, respectively. Bar = 20 μm.

669

670 **Fig. 5. Distribution of importin α1 and RAD51 in cells exposed to etoposide.**

671 (A) Schematic representation for reversine treatment followed by etoposide treatment to HeLa
672 cells. After 20 h treatment of 400 nM reversine, the cells are incubated with 10 μM etoposide for
673 6 h. (B) The ratio of the RAD51-positive MN against the DAPI-stained MN with or without
674 etoposide treatment. Signal intensities of 200 different cells in total from eight independent
675 experiments. **$P < 0.01$, two-tailed Student's t-test. error bars represent s.d. (C) IF analysis for
676 RAD51 in HeLa cells that are treated with reversine for 20 h followed by etoposide for 6 h. Two
677 images with independent cells are represented: the upper panels show MN with a low signal
678 intensity of RAD51 (Cell #1, white arrowhead), and the lower panels show MN with a high signal

679 intensity of RAD51 (Cell #2, yellow arrowhead). Bar = 10 μm. (D) IF analysis for importin α1
680 and RAD51 in HeLa cells that are treated with reversine and followed by etoposide. Two images
681 with an independent cell are represented: the upper panels (Cell #1) show MN with the high signal
682 intensity of importin α1 (green) and low intensity of RAD51 (red, yellow arrowhead), and the
683 lower panels (Cell #2) show MN with the low signal intensity of importin α1 and high signal
684 intensity of RAD51 (white arrowhead). Bar = 10 μm. (E) IF analysis for importin α1 and RAD51
685 in HeLa cells that are treated with reversine and followed by etoposide. In the upper panels (Cell
686 #1), the single cell that is indicated with a white dotted line has two MN which indicate high
687 signal intensity of importin α1 (green, yellow arrowhead) and high signal intensity of RAD51
688 (red, white arrowhead). The middle panels (Cell #2) show two MN in one cell. The below panels
689 show enlarged images that are extracted from the area enclosed by the red dotted line. The yellow
690 arrowheads indicate MN with a high signal intensity of importin α1 and low signal intensity of
691 RAD51, and the white arrowheads indicate MN with low intensity of importin α1 and high
692 intensity of RAD51. Bar = 10 μm. (F) IF analysis for RAD51 in HeLa cells are overexpressed
693 EGFP-importin α1 (EGFP-Imp-α1). HeLa cells are transfected with EGFP-Imp-α1 and followed
694 by treatment with reversine and etoposide. Two images with an independent cell are represented
695 as Cell #1 and #2. DNA is stained with DAPI. Yellow arrowheads indicate EGFP-Imp-α1
696 localized MN. The yellow line is described with X and Y in the lower panels (Cell #2) that is for
697 the fluorescence analysis in G. Bar = 10 μm. (G) Fluorescence intensities of EGFP-Imp-α1 (green),
698 RAD51 (red), and DAPI (blue) in MN are measured along with the X-Y line in F.

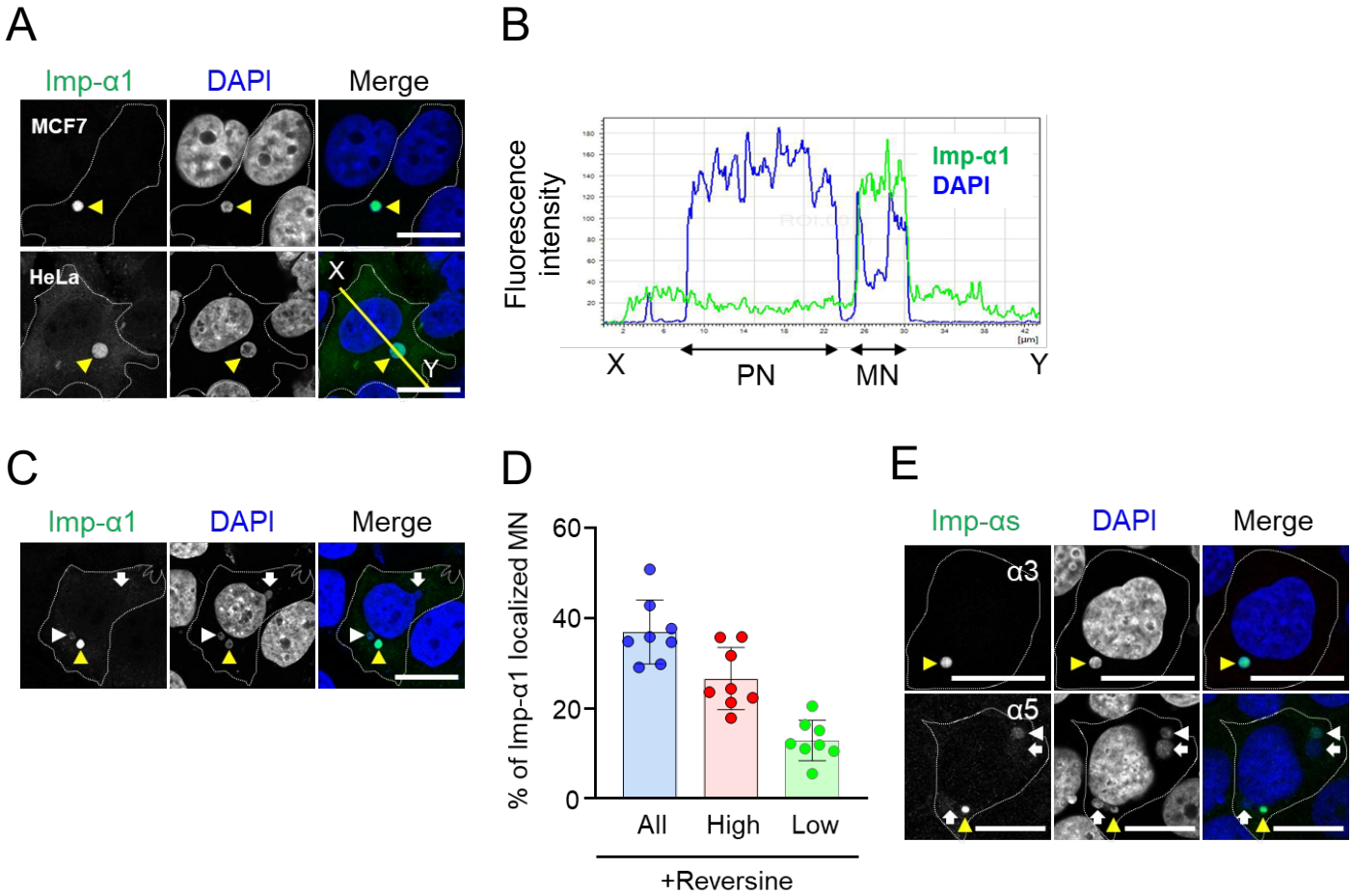

Fig. 1. Accumulation of importin α proteins in MN. (A) Exponentially growing MCF7 (upper panels) and HeLa (lower panels) cells are subjected to indirect IF analysis using an anti-importin α1 antibody (Imp-α1, left columns). White dotted lines indicate cellular boundaries. DNA is stained with DAPI (middle columns). Merged images are shown on the right. Bar = 20 μm. The yellow line described with X and Y is for fluorescence analysis in B. (B) Fluorescent intensities of importin α1 (green) and DAPI (blue) are measured along with the X-Y line in the lower right panel (HeLa cells) represented in A. PN: primary nuclei, MN: micronuclei. (C) HeLa cells are subjected to IF using an anti-importin α1 antibody. The pattern of the signals is categorized into three groups: MN with high intensity (yellow arrowhead), low intensity (white arrowhead), or no intensity (white arrow). Bar = 20 μm. (D) The ratio of the importin α1 localized-MN against the whole number of MN in HeLa cells which are treated with 400 nM reversine for 20 h. The number of DAPI-stained MN is counted and the ratio of the importin α1 positive MN is calculated (150 cells in total). Ten to fifteen cells per an observed area are counted to derive the percentage of importin α1 positive MN for eight different areas. The graph represents the category of the MN types exhibited in C. "All" (blue), "High" (red), and "Low" (green) mean either all numbers of MN with importin α1 signals, MN with the high signal intensity of importin α1, or MN with the low signal intensity of importin α1, respectively. (E) MCF7 cells are subjected to IF analysis using anti-importin α3 (upper panels) and anti-importin α5 antibodies (lower panels). The yellow arrowheads, white arrowheads, and white arrows indicate MN with either high, low or no intensity of importin αs, respectively. Bar = 20 μm.

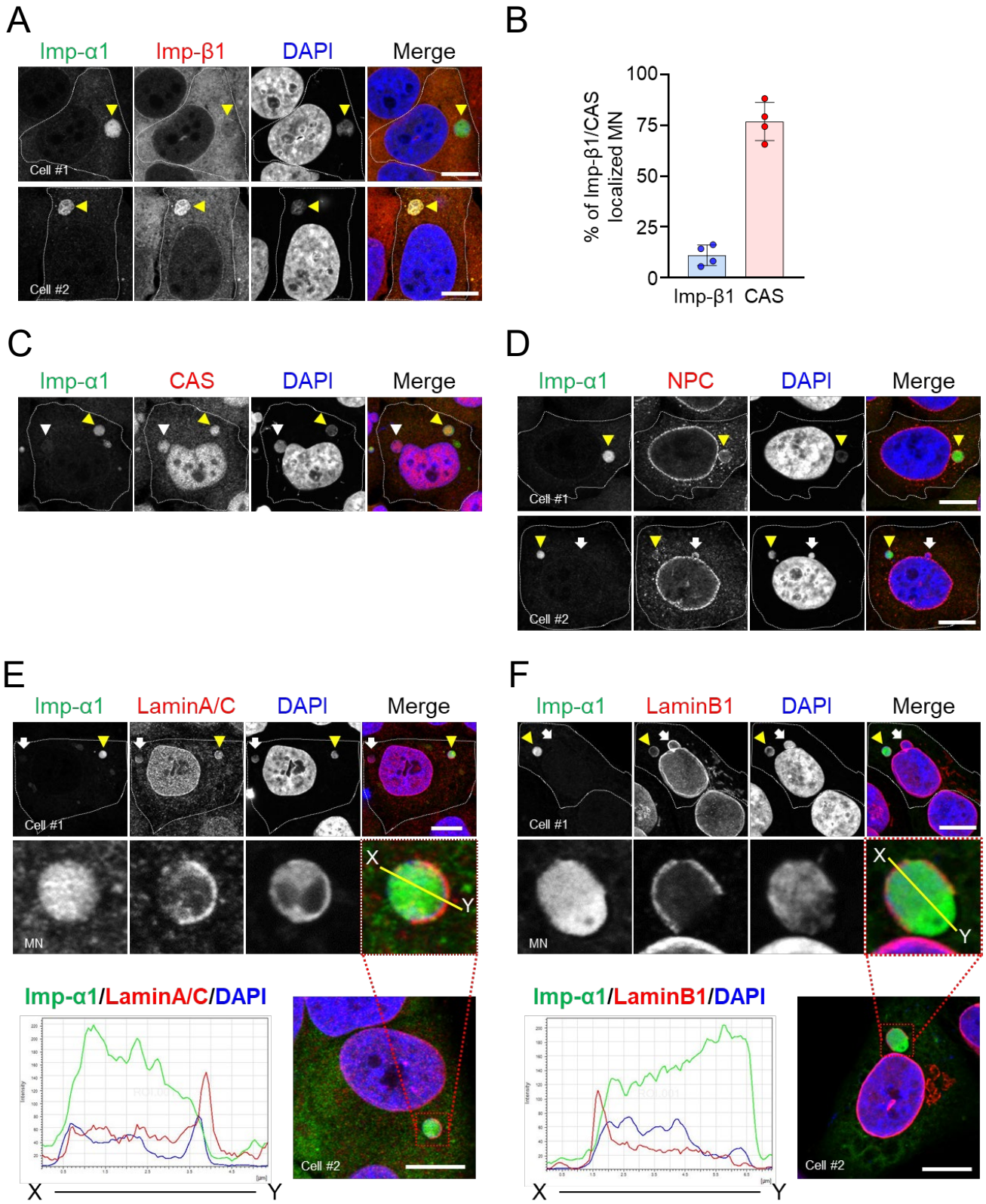
A
Imp-α1
Imp-β1
DAPI
Merge
Cell #1
Cell #2
B
% of Imp-β1/CAS localized MN
100
75
50
25
0
Imp-β1
CAS
C
Imp-α1
CAS
DAPI
Merge
D
Imp-α1
NPC
DAPI
Merge
Cell #1
Cell #2
E
Imp-α1
LaminA/C
DAPI
Merge
Cell #1
MN
X
Y
Imp-α1/LaminA/C/DAPI
Cell #2
X
Y
F
Imp-α1
LaminB1
DAPI
Merge
Cell #1
MN
X
Y
Imp-α1/LaminB1/DAPI
Cell #2
X
Y

Fig. 2. Localization of importin β1, CAS/CSE1L, and nuclear membrane proteins in importin α1-enriched MN.

(A) IF analysis of importin α1 and importin β1 in reversine-treated HeLa cells. Two images of independent cells are shown in the upper (Cell #1) and lower panels (Cell #2). DNA is stained with DAPI. Merged images are shown on the right side. White dotted lines indicate cellular boundaries. Yellow arrowhead: high intensity of importin α1 signals. Bar = 10 μm. (B) Ratio of importin β1- or CAS/CSE1L-localized-MN against the total number of MN in reversine-treated HeLa cells. The number of DAPI-stained MN (100 cells in total) is counted for independent experiments (n=4) and the ratio of importin β1- or CAS/CSE1L-positive MN is calculated. (C) MN localization of importin α1 and CAS/CSE1L in the reversine-treated HeLa cells. Yellow arrowhead: high intensity of importin α1 signals, white arrowhead: low intensity of importin α1 signals. Bar = 10 μm. (D–F) IF analysis for importin α1 and either nucleoporin (D, is shown as NPC), Lamin A/C (E), or Lamin B1 (F) in reversine-treated HeLa cells. Yellow arrowhead, high intensity of importin α1 signals; white arrow, no importin α1 signals. Bar = 10 μm. (E,F) Two images of an independent cell are shown in the upper panel (Cell #1), and the lower panels show an enlarged MN image (Cell #2). The fluorescence intensities of importin α1 (green), Lamin A/C or Lamin B1 (red), and DAPI (blue) are measured along with the X-Y line in the lower panel (Cell #2).

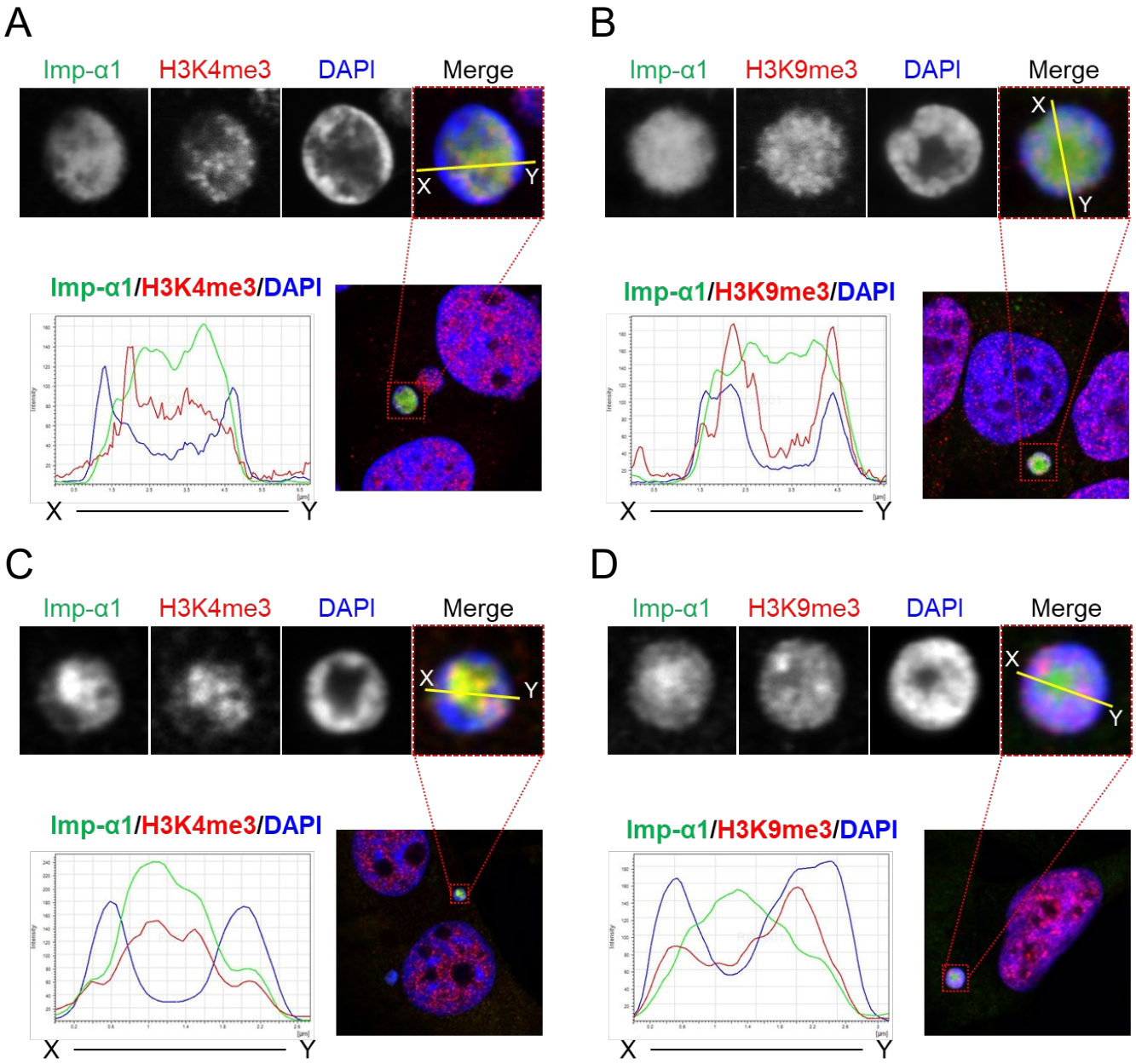

Fig. 3. Co-localization of importin α1 signals with H3K4me3 signals in MN.
(A–D) MN localization of importin α1 with H3K4me3 (A,C) or H3K9me3 (B,D) in reversine treated HeLa cells (A,B) or normally cultured MDA-MB-231 (C,D). The upper enlarged images are extracted from the area enclosed by the red dotted line in the lower image. DNA is stained with DAPI, and merged images are shown on the right side. Fluorescent intensities of importin α1 (green), modified histones (red: H3K4me3 or H3K9me3), and DAPI (blue) in MN are measured along with the X-Y line and represented in the left low. Bar = 10 μm.

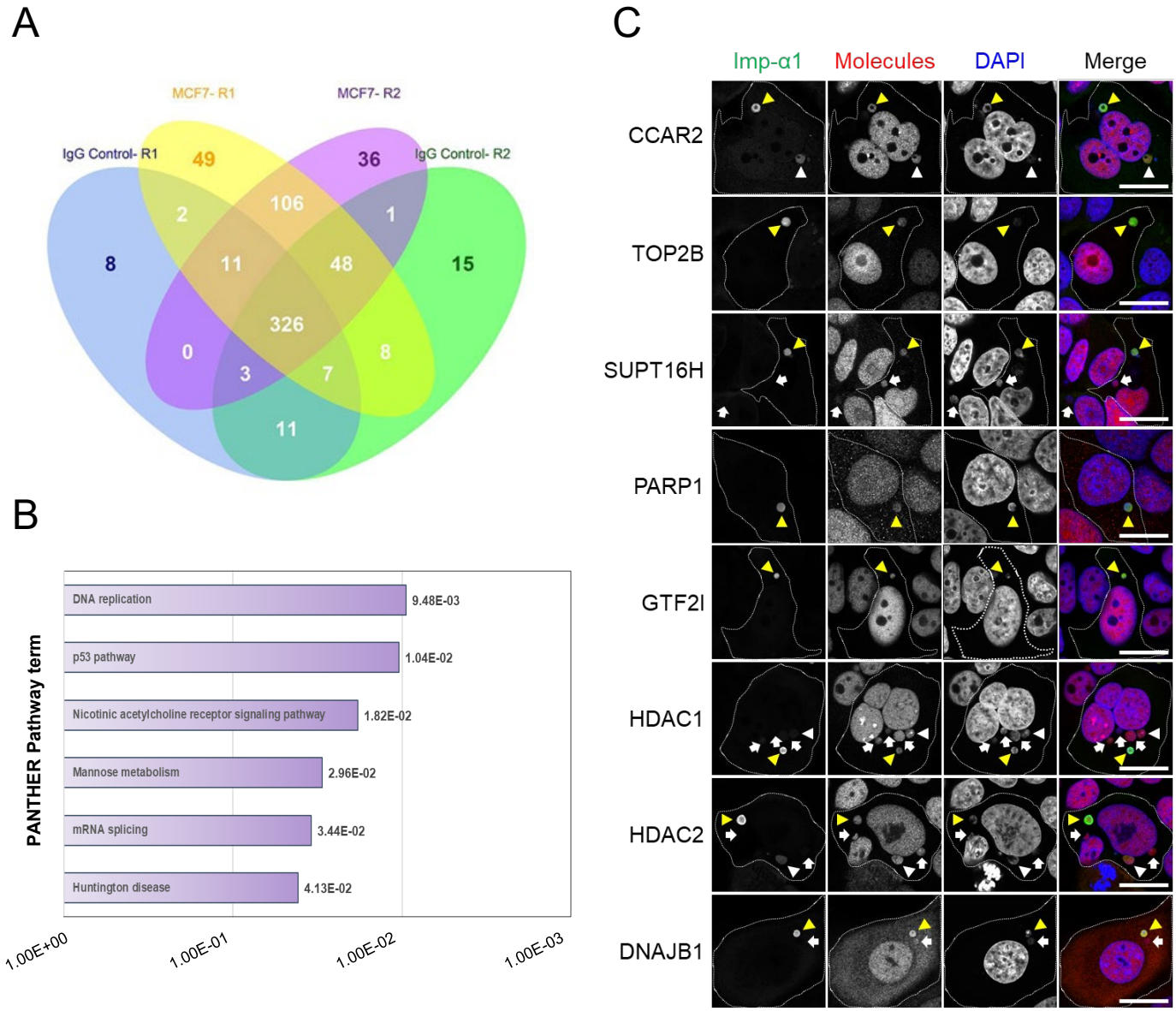

Fig. 4. Exploration of importin α1-binding proteins through the RIME analysis.
(A) Venn diagram grouping candidate importin α1-binding proteins by RIME. Two independent experiments are performed. MCF7-R1 and MCF7-R2 are proteins precipitated by anti-importin α1 antibodies, and IgG Control-R1 and -R2 are proteins precipitated by normal IgG antibodies. One hundred and six proteins are candidate binding partners of importin α1. (B) Gene Ontology analysis for identified binding proteins. All gene ontology terms are identified as a result of querying the PANTHER Pathways database for the importin α1-interacting proteins identified by RIME. Terms are ranked by p-value. (C) IF analysis for MN localization of importin α1 and candidate molecules identified by RIME in HeLa cells. Cells are treated with 400 nM reversine for 20 h, and then, the molecules described are detected by the specific antibodies. White dotted lines indicate cellular boundaries. DNA is stained with DAPI. Merged images are shown on the right side. The yellow arrowheads, white arrowheads, and white arrows indicate MN with either high intensity, low intensity, or no intensity of importin αs, respectively. Bar = 20 μm.

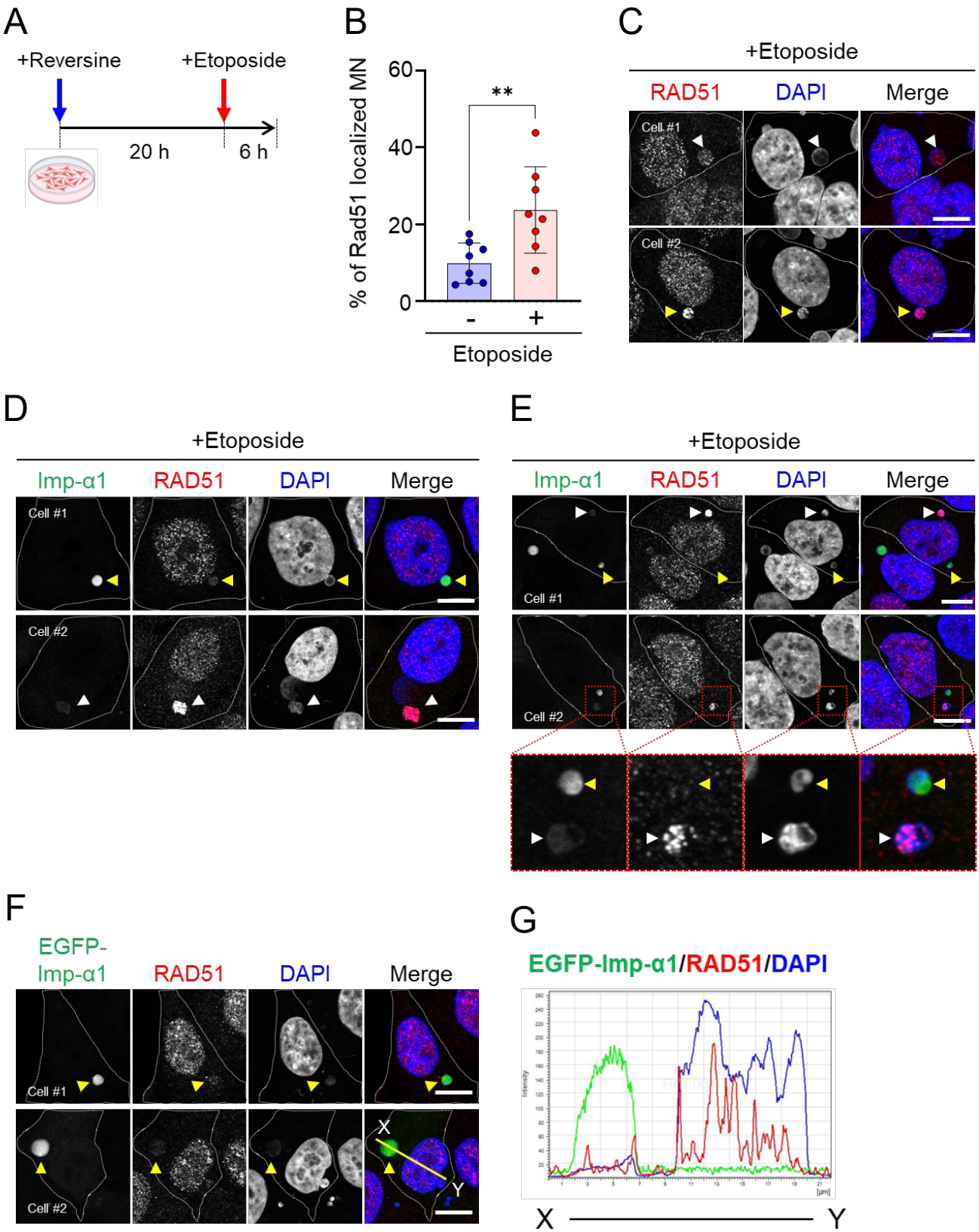
A
+Reversine
+Etoposide
20 h
6 h
B
% of Rad51 localized MN
60
40
20
0
**
-
+
Etoposide
C
+Etoposide
RAD51
DAPI
Merge
Cell #1
Cell #2
D
+Etoposide
Imp-α1
RAD51
DAPI
Merge
Cell #1
Cell #2
E
+Etoposide
Imp-α1
RAD51
DAPI
Merge
Cell #1
Cell #2
F
EGFP-Imp-α1
RAD51
DAPI
Merge
Cell #1
Cell #2
X
Y
G
EGFP-Imp-α1/RAD51/DAPI
X
Y

Fig. 5. Distribution of importin α1 and RAD51 in cells exposed to etoposide.
(A) Schematic representation for reversine treatment followed by etoposide treatment to HeLa cells. After 20 h treatment of 400 nM reversine, the cells are incubated with 10 μM etoposide for 6 h. (B) The ratio of the RAD51-positive MN against the DAPI-stained MN with or without etoposide treatment. Signal intensities of 200 different cells in total from eight independent experiments. **$P < 0.01$, two-tailed Student's t-test. error bars represent s.d. (C) IF analysis for RAD51 in HeLa cells that are treated with reversine for 20 h followed by etoposide for 6 h. Two images with independent cells are represented: the upper panels show MN with a low signal intensity of RAD51 (Cell #1, white arrowhead), and the lower panels show MN with a high signal intensity of RAD51 (Cell #2, yellow arrowhead). Bar = 10 μm. (D) IF analysis for importin α1 and RAD51 in HeLa cells that are treated with reversine and followed by etoposide. Two images with an independent cell are represented: the upper panels (Cell #1) show MN with the high signal intensity of importin α1 (green) and low intensity of RAD51 (red, yellow arrowhead), and the lower panels (Cell #2) show MN with the low signal intensity of importin α1 and high signal intensity of RAD51 (white arrowhead). Bar = 10 μm. (E) IF analysis for importin α1 and RAD51 in HeLa cells that are treated with reversine and followed by etoposide. In the upper panels (Cell #1), the single cell that is indicated with a white dotted line has two MN which indicate high signal intensity of importin α1 (green, yellow arrowhead) and high signal intensity of RAD51 (red, white arrowhead). The middle panels (Cell #2) show two MN in one cell. The below panels show enlarged images that are extracted from the area enclosed by the red dotted line. The yellow arrowheads indicate MN with a high signal intensity of importin α1 and low signal intensity of RAD51, and the white arrowheads indicate MN with low intensity of importin α1 and high intensity of RAD51. Bar = 10 μm. (F) IF analysis for RAD51 in HeLa cells are overexpressed EGFP-importin α1 (EGFP-Imp-α1). HeLa cells are transfected with EGFP-Imp-α1 and followed by treatment with reversine and etoposide. Two images with an independent cell are represented as Cell #1 and #2. DNA is stained with DAPI. Yellow arrowheads indicate EGFP-Imp-α1 localized MN. The yellow line is described with X and Y in the lower panels (Cell #2) that is for the fluorescence analysis in G. Bar = 10 μm. (G) Fluorescence intensities of EGFP-Imp-α1 (green), RAD51 (red), and DAPI (blue) in MN are measured along with the X-Y line in F.